JOURNAL OF COMPUTATIONAL PHYSICS **134,** 62–74 (1997)
ARTICLE NO. CP975652

Finite Interpolation in Green Function Deterministic Numerical Methods

S. Taddei

Dipartimento di Fisica, Università degli Studi di Firenze and Istituto Nazionale di Fisica Nucleare, Sezione di Firenze, Largo Enrico Fermi 2, I-50125, Firenze, Italy

Received December 11, 1996

An expansion on a finite set of interpolating functions is used within the framework of Green function deterministic numerical methods. Applications to some problems with one-dimensional, central, and tensor potentials are described. The precision of the numerical results is strongly improved.

INTRODUCTION

In the past two decades a great deal of effort has been devoted to solving the Schrödinger equation numerically. The need for a numerical approach can arise in many fields, from nuclear to molecular physics. The currently available numerical methods for solving the Schrödinger equation fall into two main categories: those based on the Hamiltonian approach and those related to the evolution operator. In both cases either direct diagonalization or iterative multiplication techniques can be used. In this paper we deal with methods belonging to the second category. They have been proven to have very good stability and convergence in the computation of bound states of a quantum system and high accuracy in delicate tunneling problems and in the calculation of excited levels [1–8]. Moreover, much work has been devoted to the solution of the time-dependent Schrödinger equation, namely the problem of propagating a wave packet [9–13]. Here we consider only the bound states and we use the Euclidean propagators (imaginary time formulation). This allows us to work with Gaussian, rather than oscillatory, functions and it gives a significative gain in stability and accuracy. However, the main idea could also be applied to the general case.

The method of solving the Schrödinger equation numerically starting from the evolution operator of the quantum system has its origin in the Feynman formulation of quantum mechanics. The fundamental ingredient of such a formulation is the short time propagator $K(\mathbf{x}, \mathbf{y}; \varepsilon)$, defined for an infinitesimal time interval ε. The propagator $K(\mathbf{x}, \mathbf{y}; \varepsilon)$ represents the kernel of the Schrödinger equation and contains all the information about the quantum system. Two possibilities for extracting such information are: (a) diagonalization of $K(\mathbf{x}, \mathbf{y}; \varepsilon)$ and (b) iteration of the propagator composition rule to obtain the finite time Green function and to calculate the ground state energy and wave function. These operations can be performed both by ''deterministic'' and Monte Carlo methods. The latter have the important feature of facing problems with arbitrary dimensionality (see, for instance, [14]). However, a fundamental limit is the need for high statistics, and then large CPU time, to reduce statistical errors. On the other hand deterministic methods can be very accurate and relatively fast. Here we face deterministic techniques only and we refer to the methods of type (a) and (b) as ''Green function deterministic numerical diagonalization'' (GFDND) and ''Green function deterministic numerical multiplication'' (GFDNM), respectively.

The main goal of this paper is to describe the application of the finite interpolation method, i.e., the expansion of the wave function and the propagator on a finite set of basis functions, in the framework of the GFDND and the GFDNM. We test such a method on some problems with one-dimensional, central, and tensor potentials.

The paper consists of five sections plus an Appendix. In the first section we discuss some properties of the short time propagator. In the second section we describe the numerical methods employed. The third section is devoted to the study of the propagator in the two-body problem for both central and tensor potentials. In the fourth we present some numerical results and we make a comparison with the results of a different technique based on the Hamiltonian and on a discrete variable representation method. The fifth section is the conclusion. In the Appendix we give a more formal and general treatment of the finite interpolation method.

I. SHORT TIME PROPAGATOR

The fundamental quantity in the Feynman formulation of quantum mechanics is the short time propagator $K(\mathbf{x}, \mathbf{y}; \varepsilon)$. This propagator determines the evolution of the quantum system in a small time interval ε, by relating the wave function $\psi(\mathbf{x}; t_0 + \varepsilon)$ to the wave function at time t_0

0021-9991/97 $25.00

$$\psi(\mathbf{x}; t_0 + \varepsilon) = \int K(\mathbf{x}, \mathbf{y}; \varepsilon)\psi(\mathbf{y}; t_0)\, d\mathbf{y}. \quad (1)$$

The short time propagator satisfies the semigroup composition rule

$$K(\mathbf{x}, \mathbf{y}; 2\varepsilon) = \int d\mathbf{z}\, K(\mathbf{x}, \mathbf{z}; \varepsilon)K(\mathbf{z}, \mathbf{y}; \varepsilon). \quad (2)$$

In the following we consider Euclidean propagators and ε is an imaginary time. For the sake of simplicity, we deal with only one-dimensional or radial propagators; the extension of the present analysis to several dimensions is straightforward.

The Euclidean short time propagator is given by (we use units $\hbar = m = 1$)

$$K(x, y; \varepsilon) = \frac{1}{\sqrt{2\pi\varepsilon}} \exp\left\{-\frac{1}{2\varepsilon}(x - y)^2 - f(x, y; \varepsilon)\right\}, \quad (3)$$

where the first term in the exponential corresponds to the kinetic part of the Hamiltonian, and the function $f(x, y; \varepsilon)$ is the potential term. Its explicit expression depends on the prescription chosen: for example, the last point rule $f(x, y; \varepsilon) = \varepsilon V(x)$ gives a short time propagator correct up to $O(\varepsilon)$ only, while the symmetric expression $\varepsilon[V(x) + V(y)]/2$ is correct up to $O(\varepsilon^2)$ (see, for instance, [15]). A systematic expansion of the short time propagator in ε is also possible [8, 16, 17].

We describe here two methods for obtaining the energy levels and the bound state wave functions of a quantum system.

The first method is based on Eq. (1): if E_n and $\psi_n(x)$ are respectively the eigenvalues and eigenvectors of the Hamiltonian,

$$\int K(x, y; \varepsilon)\psi_n(y)\, dy = e^{-\varepsilon E_n}\psi_n(x). \quad (4)$$

This is simply an eigenvalue integral equation. Its solution yields directly the energy levels and the wave functions of the Hamiltonian.

An alternative method relies on the path integral calculation of the finite time propagator $K(x, y; T)$ in the $T \to \infty$ limit. Let us consider the semigroup composition law (2). By iterating this rule we can get the finite time Green function starting from the short time propagator

$$K(x, y; T = (M + 1)\varepsilon) = \int \cdots \int \prod_{i=1}^{M} dx_i\, K(x, x_M; \varepsilon) \quad (5)$$
$$K(x_M, x_{M-1}; \varepsilon) \cdots K(x_1, y; \varepsilon).$$

This is basically the discretized form of the Feynman integral. From $K(x, y; T)$ we can obtain the ground state energy by using the Feynman–Kac formula (see, for example, [18])

$$E_0 = -\lim_{T\to\infty} \log \frac{Z(T)}{T}, \quad (6)$$

where

$$Z(T) = \int dx\, K(x, x; T). \quad (7)$$

Moreover, the probability density $|\psi_0(x)|^2$ is given by

$$|\psi_0(x)|^2 = -\lim_{T\to\infty} \frac{K(x, x; T)}{Z(T)}. \quad (8)$$

A disadvantage of this approach is that it yields directly only the ground state properties. On the other side it can be sometimes useful to have the finite time propagator (for example, when studying a statistical system it may be of interest to obtain the density matrix at finite temperature).

By solving the integrals in Eqs. (4) and (2) numerically, we get the energy levels and the bound state wave functions of the quantum system. We will refer to the deterministic numerical methods based on the first approach described in this section as GFDND and to those based on the second one as GFDNM. In both cases we obtain the same results for the ground state.

II. NUMERICAL METHODS

A. *Integration Rules*

In this subsection we give a brief sketch of an integration rule method used for solving Eqs. (4) and (5) numerically. More detailed discussions have already been published [1, 2, 5–8].

Equations (4) and (2) can be approximated by numerical integration rules, yielding, respectively,

$$\sum_{j=1}^{N} w_j K_{ij}^{\varepsilon}\psi(x_j) \simeq e^{-E\varepsilon}\psi(x_i), \quad (9)$$

and

$$K_{ij}^{2\varepsilon} \simeq \sum_{h=1}^{N} w_h K_{ih}^{\varepsilon} K_{hj}^{\varepsilon}, \quad (10)$$

where $K_{ij}^{\varepsilon} \equiv K(x_i, x_j; \varepsilon)$, and w_h are the weights associated with the integration rule.

Unfortunately, there are some problems. The first difficulty is in the choice of the numerical integration rule. Since the interval of integration in Eqs. (4) and (2) goes

from $-\infty$ to $+\infty$, we should use a quadrature rule for improper integrals (for instance, Gaussian quadrature). But there is a constraint: since the integrand is mainly a narrow Gaussian of width $\sqrt{\varepsilon}$ whose central position, x_i, moves on the entire interval, we need a grid dense enough to yield an accurate quadrature everywhere. Then we are forced to take a uniform distribution of grid points with a distance $\Delta x_i = x_i - x_{i-1} \sim \sqrt{\varepsilon}$. Therefore a finite number of points requires a finite range of integration, L, which corresponds to confining the system in a "box" of length L. However, if the interval is large enough, this gives negligible corrections to the energies and to the wave functions of the bound states.

In conclusion, by diagonalizing the matrix $w_j K_{ij}^{\varepsilon}$ we can obtain the energies and the wave functions of the quantum system directly. Instead, by iterating Eq. (10) and using the Feynman–Kac formula we obtain the finite time Euclidean Green function and evaluate the ground state energy and wave function. In practice the convergence is attained in a few iterations.

B. *Finite Interpolation*

Actually, in the previous method there are two problems: the dependence between ε and Δx and the finite range of integration, L. Obviously they are related: if we fix the number of grid points and the interval L, then the value of ε is fixed by the relation $\varepsilon \sim \Delta x^2$ (in practice, a ratio $\varepsilon/\Delta x^2 = 1$ gives an accuracy greater than 1% and already with 1.25 we get at least eight digits). In other words, if we take ε tending to zero the kinetic energy part of the propagator becomes strongly peaked and we need a very large number of points to obtain a good precision. This means that we cannot take ε as small as possible and the systematic error which depends on ε can be quite large (this systematic error should not be confused with the numerical error in the quadrature, which depends only on the ratio $\varepsilon/\Delta x^2$).

These problems can be overcome by using an alternative method. In the following we give a heuristic and simplified description of this technique. A more formal and general treatment will be given in the Appendix.

The method is based on the expansion of the unknown wave function $\psi_n(x)$ on some basis of interpolating functions $\varphi_i(x)$ [19]

$$\psi_n(x) \simeq \sum_{i=1}^{N} a_i^n \varphi_i(x). \tag{11}$$

Since $\psi_n(x)$ is usually smooth we can attain good accuracy with quite small N. This technique can be used within both the GFDND and the GFDNM. Let us start from the GFDND and take the interpolating functions to be Lagrange polynomials. Then Eq. (11) becomes

$$\psi_n(x) \simeq \sum_{i=1}^{N} \psi_i^n l_i(x), \tag{12}$$

where now the coefficients ψ_i^n are just the values of the function $\psi_n(x)$ in the interpolating points x_i. The substitution of $\psi_n(x)$ in Eq. (4) yields

$$\int K(x, y; \varepsilon) \sum_{i=1}^{N} \psi_i^n l_i(y)\, dy \simeq e^{-\varepsilon E_n} \psi_n(x). \tag{13}$$

Since the functions $\varphi_i(x)$ are given, we can calculate the integrals

$$\tilde{K}_i(x; \varepsilon) = \int K(x, y; \varepsilon) l_i(y)\, dy, \tag{14}$$

and Eq. (13) becomes

$$\sum_{i=1}^{N} \psi_i^n \tilde{K}_i(x; \varepsilon) \simeq e^{-\varepsilon E_n} \psi_n(x). \tag{15}$$

We can find the coefficients ψ_i^n by selecting N distinct points x_i and by solving the following system of $N \times N$ linear equations (collocation method)

$$\sum_{j=1}^{N} \psi_j^n \tilde{K}_{ij}^{\varepsilon} = e^{-\varepsilon E_n} \psi_i^n, \tag{16}$$

where

$$\tilde{K}_{ij}^{\varepsilon} \equiv \tilde{K}_j(x_i; \varepsilon). \tag{17}$$

Then we have the usual eigenvalue problem, like in Eq. (9).

Now we apply the finite interpolation technique to the case of the GFDNM. Let us start from the equation

$$\begin{aligned} &\int K(x, y; 2\varepsilon) \psi(y)\, dy \\ &\qquad = \iint K(x, z; \varepsilon) K(z, y; \varepsilon) \psi(y)\, dz\, dy. \end{aligned} \tag{18}$$

By substituting the expansion (12) and integrating, we obtain

$$\sum_{j=1}^{N} \tilde{K}_j(x; 2\varepsilon) \psi_j = \int \sum_{j=1}^{N} K(x, z; \varepsilon) \tilde{K}_j(z; \varepsilon) \psi_j\, dz. \tag{19}$$

The function $\tilde{K}_j(z; \varepsilon)$ is a convolution of a narrow Gaussian with a smooth function, and it is also smooth; therefore we can expand it as

$$\tilde{K}_j(z;\varepsilon) \simeq \sum_{h=1}^{N} \tilde{K}^{\varepsilon}_{hj} l_h(z). \tag{20}$$

By integrating again we have

$$\sum_{j=1}^{N} \tilde{K}^{2\varepsilon}_{ij}\psi_j \sum_{j=1}^{N}\sum_{h=1}^{N} \tilde{K}^{\varepsilon}_{ih}\tilde{K}^{\varepsilon}_{hj}\psi_j, \tag{21}$$

and by comparing the coefficients we obtain the composition rule

$$\tilde{K}^{2\varepsilon}_{ij} = \sum_{h=1}^{N} \tilde{K}^{\varepsilon}_{ih}\tilde{K}^{\varepsilon}_{hj}. \tag{22}$$

This rule is formally equal to that of Eq. (10), and we can proceed as before. By iterating Eq. (22) we get the finite time matrix $\tilde{K}^{T}_{ij}$. Moreover, as shown in the Appendix, we have

$$\int K(x,x;T)\,dx \simeq \sum_{i=1}^{N} \tilde{K}^{T}_{ii}. \tag{23}$$

Therefore we can obtain the ground state energy by the Feynman–Kac formula, and the matrix elements $\tilde{K}^{T}_{ij}$ contain information about the ground state wave function (see Eq. (A26) in the Appendix).

The main point of these new methods is that the integrals in Eq. (14) can be calculated with any accuracy by analytic or numerical methods. As a consequence the value of ε is not related to the choice of the points x_i anymore. Therefore we have three important results.

First of all we can now take the time step, ε, very small and the systematic error depending on it can be reduced.

As a second result we can choose an appropriate distribution of grid points according to the shape of the wave functions and we can obtain a better accuracy with the same number of points. This is equivalent to saying that we can choose an appropriate transformation of variables which maps the original interval of integration into a new one and then discretize the new variable. In particular, we can map the infinite interval into a finite one. So we have the advantage of taking correctly into account the boundary conditions simply by requiring that the wave functions vanish in the extremes of the interval.

The third result concerns the choice of the prescription for the potential part of the propagator, i.e., the function $f(x, y; \varepsilon)$. Since the value of ε can now be taken very small we can choose any rule. In particular, if we adopt the last-point rule, $f(x, y; \varepsilon) = \varepsilon V(x)$, the potential term can be put out of the integral. This has two consequences: first, the integrals in Eq. (14) could be often worked out analytically (although this can be inconvenient, since the numerical computation is usually quite fast and accurate). Second, and most important, if the mass does not depend on the position the matrix of the propagator in the multidimensional case can be factorized as a tensorial product of one-dimensional free propagator matrices multiplied by the diagonal matrix corresponding to the potential term. This means that if we solve the eigenvalue problem by iterative techniques (for instance, the Lanczos method [20]) we need much less effort in terms of both computation and memory requirements. Then it becomes possible to deal with three- or four-dimensional problems.

III. CENTRAL AND TENSOR POTENTIALS

The previous discussion is limited to one-dimensional systems. We now consider three-dimensional systems with central and tensor potentials. These can be reduced, by a separation of the angular variables, to one-dimensional problems; but a fundamental difference arises in the expression of short time propagators. This difference is illustrated in the next section.

A. *Central Potentials*

Let us consider a three-dimensional problem with a central potential. In this case we can separate the angular and the radial variables and the propagator factorizes in the following way [21],

$$K(\mathbf{r}, t; \mathbf{r}_0, t_0) = \sum_{l=0}^{\infty}\sum_{m=-l}^{l} \frac{1}{rr_0} g_l(r, t; r_0, t_0)\, Y_{lm}(\theta,\phi) Y^{*}_{lm}(\theta_0, \phi_0), \tag{24}$$

where $Y_{lm}(\theta, \phi)$ are the spherical harmonics. The contribution of states with angular momentum l is

$$\begin{aligned} K_l(\mathbf{r}, t; \mathbf{r}_0, t_0) &= \langle \mathbf{r}|\hat{P}_l e^{-\hat{H}(t-t_0)}\hat{P}_l|\mathbf{r}_0\rangle \\ &= \sum_{m=-l}^{l} \frac{1}{rr_0} g_l(r, t; r_0, t_0)\, Y_{lm}(\theta,\phi) Y^{*}_{lm}(\theta_0, \phi_0). \end{aligned} \tag{25}$$

Obviously, since the system has spherical symmetry, the contributions corresponding to different values of l are separated. If we consider the radial wave function $R_{nl}(r)$, it satisfies the integral equation

$$\int g_l(r, \varepsilon; r', 0) R_{nl}(r')\,dr' = e^{-\varepsilon E_{nl}} R_{nl}(r). \tag{26}$$

Moreover the radial propagators $g_l(r, t; r_0, t_0)$ obey the usual composition law

$$g_l(r, t; r_0, t_0) = \int dr'\, g_l(r, t; r', t') g_l(r', t'; r_0, t_0), \quad (27)$$

and they are given by

$$g_l(\mathbf{u}) = k_l(\mathbf{u}) \exp\{-f(\mathbf{u})\}, \quad (28)$$

where $\mathbf{u} \equiv (r, \varepsilon; r_0, 0)$; $f(\mathbf{u})$ depends, as usual, on the prescription chosen for the potential and

$$k_l(\mathbf{u}) = \frac{1}{\sqrt{2\pi\varepsilon}} \sqrt{2\pi \frac{rr_0}{\varepsilon}}\, \varepsilon^{-rr_0/\varepsilon} I_{l+1/2}\left(\frac{rr_0}{\varepsilon}\right) e^{-(r-r_0)^2/2\varepsilon}, \quad (29)$$

where $I_{l+1/2}(z)$ are the modified Bessel functions. As in the one-dimensional case this short time propagator can be used to obtain the finite time propagator, the binding energies, and the wave functions of the system.

B. *Tensor Potential* (*Deuteron*)

A more sophisticated system is the deuteron, with the two nucleons interacting through a realistic potential, which also has a tensor part that does not commute with the orbital angular momentum. The Hamiltonian can be written in the following way,

$$\hat{H} = -\frac{1}{2r^2}\frac{\partial}{\partial r}\left(r^2 \frac{\partial}{\partial r}\right) + \frac{\hat{l}^2}{2r^2} + V_C(r) + \hat{O}_{L,S} V_{L,S}(r) + V_T(r)\hat{S}_{12}(\theta, \phi), \quad (30)$$

where $\hat{O}_{L,S}$ represents the spin and the orbital angular momentum operators, and $\hat{S}_{12}$ is the tensor operator. The partial Euclidean propagator of the deuteron is

$$K_{JW}(\mathbf{r}, \sigma, t; \mathbf{r}_0, \sigma_0, t_0) = \langle \mathbf{r}, S, \sigma | \hat{P}_J \hat{P}_W e^{-\hat{H}(t-t_0)} \hat{P}_J \hat{P}_W | \mathbf{r}_0, S, \sigma_0 \rangle, \quad (31)$$

where $\hat{P}_J$ is the projector on states with total angular momentum J, and $\hat{P}_W$ the projector on states with parity W. By inserting into this expression a complete set of eigenvectors of the Hamiltonian (30), $|\beta, J, J_z, S, W\rangle$, we get

$$K_{JW}(\mathbf{r}, \sigma, t; \mathbf{r}_0, \sigma_0, t_0) = \sum_{\beta, J_z} \langle \mathbf{r}, S, \sigma | \beta, J, J_z, S, W \rangle \langle \beta, J, J_z, S, W | \mathbf{r}_0, S, \sigma_0 \rangle e^{-E_\beta (t-t_0)}. \quad (32)$$

The ground state of deuteron has $J = 1$, $W = +$, and $S = 1$. Furthermore, since the ground state level displays a threefold degeneracy, corresponding to the different values of J_z, it is sufficient to take into account only the contribution with $J_z = 0$. By expanding the eigenvectors of $\hat{H}$ in terms of eigenvectors of the orbital angular momentum, the propagator (31) can be written as

$$\begin{aligned}\langle \mathbf{r}, S, \sigma | \hat{P}_J \hat{P}_W e^{-\hat{H}(t-t_0)} \hat{P}_J \hat{P}_W | \mathbf{r}_0, S, \sigma_0 \rangle &= \frac{1}{rr_0} \{ g^{00}(r, t; r_0, t_0) \delta_{\sigma 0} \delta_{0\sigma_0} Y_{00}(\theta, \phi) Y^*_{00}(\theta_0, \phi_0) \\ &+ g^{02}(r, t; r_0, t_0) \delta_{\sigma 0} C^{10}_{2-\sigma_0 1\sigma_0} Y_{00}(\theta, \phi) Y^*_{2-\sigma_0}(\theta_0, \phi_0) \\ &+ g^{20}(r, t; r_0, t_0) C^{10}_{2-\sigma 1\sigma} \delta_{0\sigma_0} Y_{2-\sigma}(\theta, \phi) Y^*_{00}(\theta_0, \phi_0) \\ &+ g^{22}(r, t; r_0, t_0) C^{10}_{2-\sigma 1\sigma} C^{10}_{2-\sigma_0 1\sigma_0} Y_{2-\sigma}(\theta, \phi) Y^*_{2-\sigma_0}(\theta_0, \phi_0) \}\end{aligned} \quad (33)$$

where $C^{JM}_{LmS\sigma}$ are the Clebsch–Gordan coefficients and the g^{ab} are functions of the radial coordinates only. Therefore the tensor potential couples the two channels $l = 0$ and $l = 2$. If we write now the deuteron wave function in terms of the S and D state radial wave functions $u_\beta(r)$ and $w_\beta(r)$, we get

$$\langle \mathbf{r}, 1, \sigma | \beta, 1, 0, 1, + \rangle = \frac{u_\beta(r)}{r} \delta_{0\sigma} Y_{00}(\theta, \phi) + \frac{w_\beta(r)}{r} C^{10}_{2-\sigma 1\sigma} Y_{2-\sigma}(\theta, \phi). \quad (34)$$

It is convenient to define the matrix

$$G(\mathbf{u}) = \begin{pmatrix} g^{00} & g^{02} \\ g^{20} & g^{22} \end{pmatrix}, \quad (35)$$

and the two-component vector (u_β, w_β); then

$$\int G(r, \varepsilon; r', 0) \begin{pmatrix} u_\beta(r') \\ w_\beta(r') \end{pmatrix} dr' = e^{-\varepsilon E_\beta} \begin{pmatrix} u_\beta(r) \\ w_\beta(r) \end{pmatrix}. \quad (36)$$

Moreover the matrix G satisfies the usual composition law

$$G(r, t; r_0, t_0) = \int dr'\, G(r, t; r', t') G(r', t'; r_0, t_0), \quad (37)$$

where GG is now a matrix product. By substituting the expression (34) into Eq. (32), and comparing with Eq. (33), we obtain the relations

$$g^{00}(r, T; r_0, 0) = \sum_\beta u_\beta(r) u^*_\beta(r_0) e^{-E_\beta T}, \quad (38a)$$

$$g^{02}(r, T; r_0, 0) = \sum_\beta u_\beta(r) w^*_\beta(r_0) e^{-E_\beta T}, \quad (38b)$$

$$g^{20}(r, T; r_0, 0) = \sum_\beta w_\beta(r) u^*_\beta(r_0) e^{-E_\beta T}, \quad (38c)$$

$$g^{22}(r, T; r_0, 0) = \sum_\beta w_\beta(r) w^*_\beta(r_0) e^{-E_\beta T} \quad (38d)$$

involving the S and D components of the wave function.

Hence the radial propagator $G(r, t; r_0, t_0)$ satisfies relations which are equivalent to those of the one-dimensional case. Therefore we can recover the energy and wave function of the ground state either by using a generalization of the Feynman–Kac formula

$$E_0 = -\lim_{T\to\infty} \log \frac{Z(T)}{T}, \tag{39}$$

with

$$Z(T) = \int dr[g^{00}(r, T; r, 0) + g^{22}(r, T; r, 0)], \tag{40}$$

and

$$|u_0(r)|^2 = -\lim_{T\to\infty} \frac{g^{00}(r, T; r, 0)}{Z(T)}, \tag{41a}$$

$$|w_0(r)|^2 = -\lim_{T\to\infty} \frac{g^{22}(r, T; r, 0)}{Z(T)}, \tag{41b}$$

or by diagonalizing directly the matrix in Eq. (35).

All we need in both cases is to evaluate the short time radial propagators $g^{ab}(r, \varepsilon; r_0, 0)$. Let us start by writing the projector $\hat{P}_J \hat{P}_W$ as

$$\hat{P}_J \hat{P}_W = \int dp \sum_{S,J_z} \sum_{l_{\text{even}}} |pl\, S\, J\, J_z\rangle\langle pl\, S\, J\, J_z|, \tag{42}$$

where p is the magnitude of the momentum vector. By inserting this expression into Eq. (31), setting $J = 1$, $W = +$, $S = 1$, and taking the contribution of $J_z = 0$ only, we obtain

$$K_{JW}(\mathbf{r}, \sigma, \varepsilon; \mathbf{r}_0, \sigma_0, 0) = \int dp \sum_{l=0,2} \langle \mathbf{r}, 1, \sigma|pl\,1\,1\,0\rangle e^{-(1/2)p^2\varepsilon} \langle pl\,1\,1\,0|e^{-\hat{V}\varepsilon}|\mathbf{r}_0, S, \sigma_0\rangle. \tag{43}$$

Since the tensor operator $\hat{S}_{12}$ is a function of the angular variables, now the separation of the angular and the radial coordinates is not as straightforward as in the case of the radial potential. This difficulty can be overcome by using the fact that the exponential of the tensor potential can be written as

$$e^{\alpha \hat{S}_{12}} = A(\alpha) + B(\alpha)\hat{S}_{12}, \tag{44}$$

where

$$A(\alpha) = \tfrac{1}{5}(2e^{2\alpha} + e^{-4\alpha}), \tag{45a}$$

$$B(\alpha) = \tfrac{1}{6}(e^{2\alpha} - e^{-4\alpha}). \tag{45b}$$

Furthermore

$$\langle \mathbf{r}, 1, \sigma|\hat{S}_{12}|pl\,1\,1\,0\rangle = \sqrt{\frac{2}{\pi}} \int dr'\, pr'\, j_l(pr') \langle \mathbf{r}, 1, \sigma|\hat{S}_{12}|r'\, l\,1\,1\,0\rangle, \tag{46}$$

and

$$\hat{S}_{12}\,|r011M\rangle = \sqrt{8}\,|r211M\rangle, \tag{47a}$$

$$\hat{S}_{12}\,|r211M\rangle = \sqrt{8}\,|r011M\rangle - 2\,|r211M\rangle. \tag{47b}$$

By substituting into Eq. (43), and comparing with Eq. (33), we obtain

$$g^{00}(\mathbf{u}) = k_0(\mathbf{u})\, e^{-f_C(\mathbf{u})} A(\alpha), \tag{48a}$$

$$g^{02}(\mathbf{u}) = \frac{\sqrt{8}}{2}[k_0(\mathbf{u}) + k_2(\mathbf{u})] e^{-f_C(\mathbf{u}) - (1/2) f_{LS}(\mathbf{u})} B(\alpha), \tag{48b}$$

$$g^{20}(\mathbf{u}) = \frac{\sqrt{8}}{2}[k_0(\mathbf{u}) + k_2(\mathbf{u})] e^{-f_C(\mathbf{u}) - (1/2) f_{LS}(\mathbf{u})} B(\alpha), \tag{48c}$$

$$g^{22}(\mathbf{u}) = k_2(\mathbf{u}) e^{-f_C(\mathbf{u}) - f_{LS}(\mathbf{u})} \{A(\alpha) - 2B(\alpha)\}, \tag{48d}$$

where $\alpha = -f_T(\mathbf{u})$.

IV. RESULTS

In this section we discuss the results obtained by the finite interpolation method for some specific one-dimensional, central, and tensor potentials. However, before focusing on concrete examples, we need to make some further remarks.

First of all we must choose a set of approximating functions. In the following we use piecewise polynomials of order n even. More precisely, since high-order Lagrange polynomials may lead to unwanted oscillations, we take only the piece between the two central interpolation points. Then we repeat the process over all inner points, while the initial and final points are interpolated by the left and right side of the Lagrange polynomials, respectively. In this way we obtain a quasi-smooth interpolation. We have tested the convergence of the results by increasing n and we found a good stability. Clearly other choices (for instance, splines) can be valid as well.

The second step is the choice of a transformation of variables which maps the infinite interval into a finite one. We choose a transformation suggested in Ref. [22], which has been proven to work very well. Such a transformation maps the interval $[0, \infty)$ onto $[0, 1)$ and it is given by

$$\rho = 1 - e^{-\lambda r}, \tag{49}$$

TABLE I

Parameters of the Morse Curve

$D = 0.1744$ (a.u.)
$\beta = 1.02764$ (a.u.)
$x_e = 1.40201$ (a.u.)
$m = 918.491$ (a.u.)

where r is the original variable and ρ the new one. The parameter λ can be varied to optimize the accuracy of the numerical solution. We notice that an arbitrary parameter is introduced also in other approaches, as some kind of cutoff or interval length. It will be shown in what follows that the results are stable for a large range of values of λ (see also Ref. [22]). The value of λ must not be too large, in order not to lose accuracy in the interpolation of the tail of the wave function. On the other hand it must not be too small in order to have as many grid points as possible near the origin, where the wave function and the potential change rapidly. More precisely λ must be chosen in such a way that the grid points are distributed on the entire interval where the wave functions are significantly different from zero. In practice, this condition can be satisfied by looking at the plots of the wave functions. The correctness of the value of λ can be checked by testing the stability of the results.

Let us now analyze the numerical results obtained by using the finite interpolation within the GFDND and GFDNM. We use the prescription $f(x, y; \varepsilon) = \varepsilon V(x)$ and the integrals in Eq. (14) are computed numerically.

As a first example we consider the Morse potential given by

$$V(x) = D[1 - \exp\{-\beta(x - x_e)\}]^2. \tag{50}$$

The parameters of the Morse curve and the mass are given in Table I. In order to compare our results to those obtained by other methods, in particular the Fourier grid Hamiltonian (FGH) method [23] which is a special case of a discrete variable representation (DVR) method [24], we use the same parameters as those in Ref. [23].

The Morse potential is one-dimensional and we use the propagator given in Eq. (3), but we can still adopt the transformation given in Eq. (49). In fact, due to the hard core of the Morse potential, the wave functions are different from zero only on the positive semi-axis.

In Table II we show the results of our method compared to those in Ref. [23] and to the analytic values. We can see that the results of the GFDND are better than those of the FGH method up to the last two energy levels. Moreover we must point out that we have used the same value of the parameter λ to obtain all energy levels. If we use a more appropriate value for each wave function, the precision of our results can be even better. In Fig. 1 we compare the computed and analytic eigenfunctions obtained with 129 grid points corresponding to quantum numbers $\nu = 0$, 5, and 15. The dots represent the numerical values, while the solid lines are the analytic solutions. The wave functions are superimposed on the Morse potential with the zero of the wave functions placed at the bound state energies. Both the numerical and the analytic wave functions have been normalized. The differences between them are nowhere discernible to the resolution of the plots (see also Ref. [23]).

Let us now discuss in detail the convergence and the stability of the method. In order to obtain such high accuracy we use polynomials of order 20. The results do not change significantly by using higher degrees.

The stability in λ is shown in Figs. 2 and 3 for 65 and 129 grid points, respectively. The numerical values of four different energy levels are plotted versus the parameter λ. The plots show that for higher quantum numbers, ν, we should use smaller values of λ. This is obvious since if the wave functions are less confined the distribution of grid points must be larger. The results of Table II are obtained with $\lambda = 0.3$ (a.u.), which is a good value for almost all energy levels. As a last remark we note that by increasing the number of points, the stability increases as well.

Finally, in Table III we report the convergence of the numerical values with respect to the time step ε. The results previously discussed in Table II were obtained with $\varepsilon = 1 \times 10^{-4}$, which gives enough accuracy. In fact, we can see in Table III that it is possible to attain even more precision.

As a second example let us consider the spherically symmetric Pöschl–Teller potential given by

$$V(r) = V_0 \tanh^2(r). \tag{51}$$

The energy levels with angular momentum $l = 0$ of such a potential are known analytically. In Table IV we compare our numerical results with the analytic ones. The parameter λ has been taken in the range of stability and the time step ε has been fixed to obtain the required accuracy. The data show that good precision is attained with a relatively small number of grid points.

As a further example let us consider another potential with analytic solutions:

$$V(r) = \frac{A}{r^2} - \frac{1}{r} \tag{52}$$

(Krazer potential). In Table V we report the results for the ground state energy of such a potential with different values of the parameter A. The agreement between the numerical and analytic calculations is excellent, even for small A (cf. the results of [6]).

TABLE II

Comparison of the Energy Values (a.u.) for the Morse Potential Calculated by Using the GFDND, the Fourier Grid Hamiltonian Method, and the Exact Analytic Formula

	Fourier grid Hamiltonian method		Green function deterministic numerical diagonalization		
ν	$N = 65$	$N = 129$	$N = 65$	$N = 129$	Exact
0	0.00986923	0.00986923	0.00986922	0.00986922	0.00986922
1	0.02874536	0.02874536	0.02874535	0.02874535	0.02874535
2	0.04647171	0.04647173	0.04647172	0.04647172	0.04647172
3	0.06304833	0.06304835	0.06304834	0.06304832	0.06304833
4	0.07847564	0.07847520	0.07847524	0.07847517	0.07847518
5	0.09275367	0.09275229	0.09275247	0.09275226	0.09275227
6	0.10587909	0.10587962	0.10588013	0.10587959	0.10587960
7	0.11784686	0.11785719	0.11785832	0.11785716	0.11785717
8	0.12866157	0.12868500	0.12868717	0.12868497	0.12868498
9	0.13834083	0.13836306	0.13836673	0.13836302	0.13836303
10	0.14689650	0.14689135	0.14689693	0.14689131	0.14689132
11	0.15431741	0.15426987	0.15427749	0.15426984	0.15426985
12	0.16057903	0.16049864	0.16050793	0.16049862	0.16049862
13	0.16566518	0.16557765	0.16558795	0.16557763	0.16557763
14	0.16957779	0.16950690	0.16953042	0.16950689	0.16950689
15	0.17233036	0.17228639	0.17263242	0.17228666	0.17228638
16	0.17394440	0.17391637	0.17589464	0.17397072	0.17391611

Note. The degree of the Lagrange polynomial is 20. The parameter λ is 0.3 (a.u.). The time step ε is 1×10^{-4} (a.u.).

We note that the expression in Eq. (29) of the short time propagator is not correct for singular potentials [21]. However, since the wave function is almost zero near the origin, the contributions to the integral coming from such a region are very small, and we still obtain good numerical results (see Table VI). The convergence of the numerical values toward the analytic ones is shown by increasing the number of grid points.

The last example is the problem of the deuteron with a realistic nuclear potential, which includes a tensor part. In particular we use the Argonne V14 potential [25]. This system is difficult to study, because the very long tail of the wave function requires a large number of points in order to attain good precision. The finite interpolation method gives excellent results, as shown in Table VII (cf. [6]). In Fig. 4 we show how the numerical values of the energy change by varying the parameter λ with a fixed number of points. If λ is taken in the appropriate interval, according to the previous discussions, the results are stable. Obviously the stability increases if we take a larger number of points (the plot in Fig. 4 has been made with only 50 points). However, since in the deuteron case it is important to have many grid points in the region $r < 1$ fm, a transformation more efficient than (49) could be used [26].

V. CONCLUSIONS

In this paper we have applied the finite interpolation method to the GFDND and the GFDNM. We have three main results:

i. We can reduce the systematic error due to the finite time step ε without increasing the number of grid points.

ii. We can perform any change of variables and integrate on the entire real axis. This means also that we can choose an appropriate distribution of grid points according to the shape of the wave function so as to obtain higher precision with the same number of points.

iii. We can find a tensorial representation of the multidimensional propagator which permits a reduction in the computational and memory requirements.

These improvements allow us to remarkably increase the efficiency of Green function deterministic numerical methods.

APPENDIX

In general the problem of interpolation can be formulated as follows [27]:

Let X be a linear space of dimension N and let L_1, L_2, ..., L_N be N given linear functionals defined on X. For a given set of values $w_1, w_2, ..., w_N$, can we find an element of X, say φ, such that

$$L_i[\varphi] = w_i, \quad i = 1, 2, ..., N? \tag{A1}$$

This is possible if, given N independent elements φ_1, φ_2, ..., φ_N of X, the following holds:

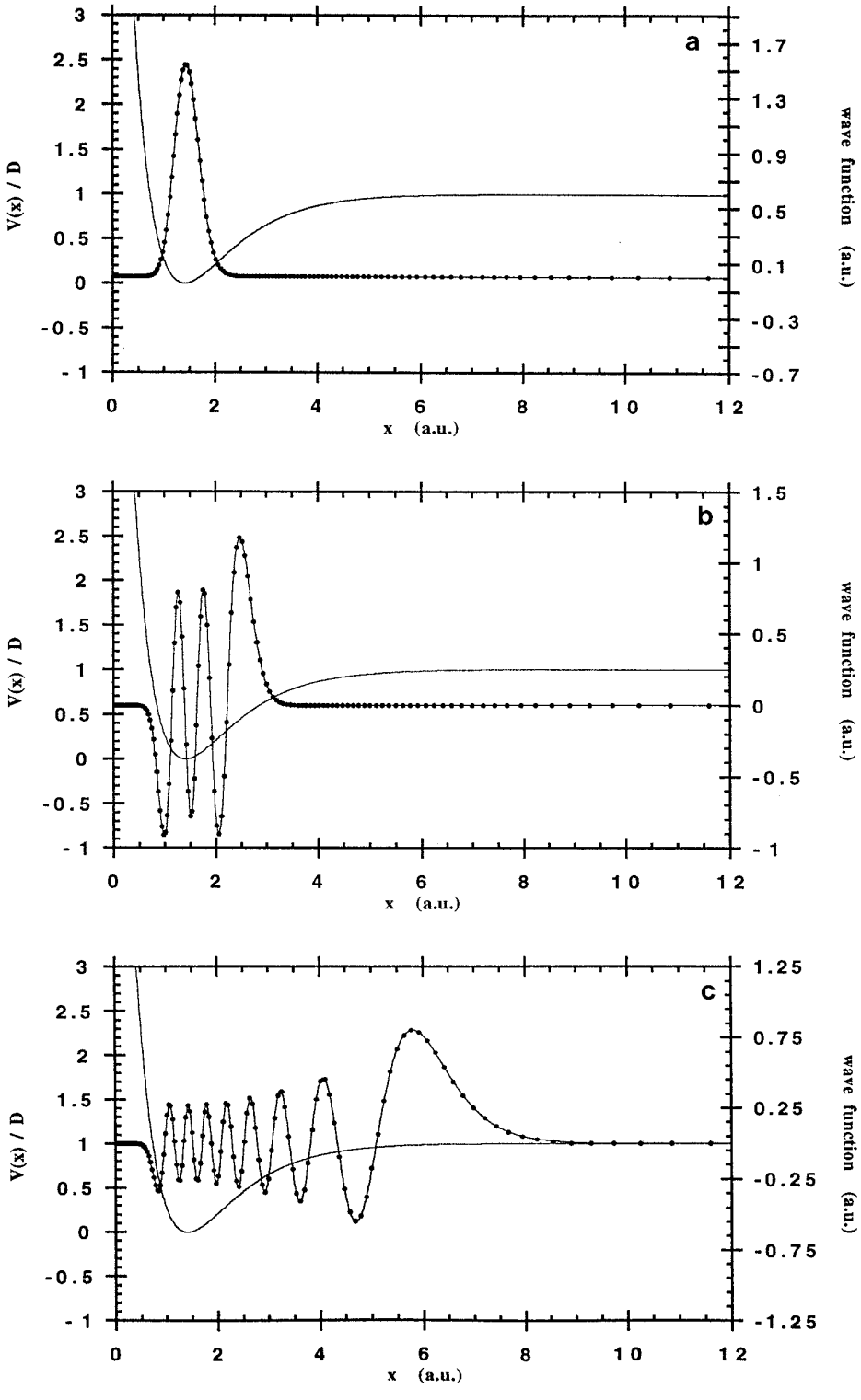

FIG. 1. Comparison of analytic (solid line) and numerically computed (dots) eigenfunctions for the $\nu = 0$ (a), 5 (b), and 15 (c) states of the Morse potential (129 grid points). The wave functions are superimposed on the Morse potential.

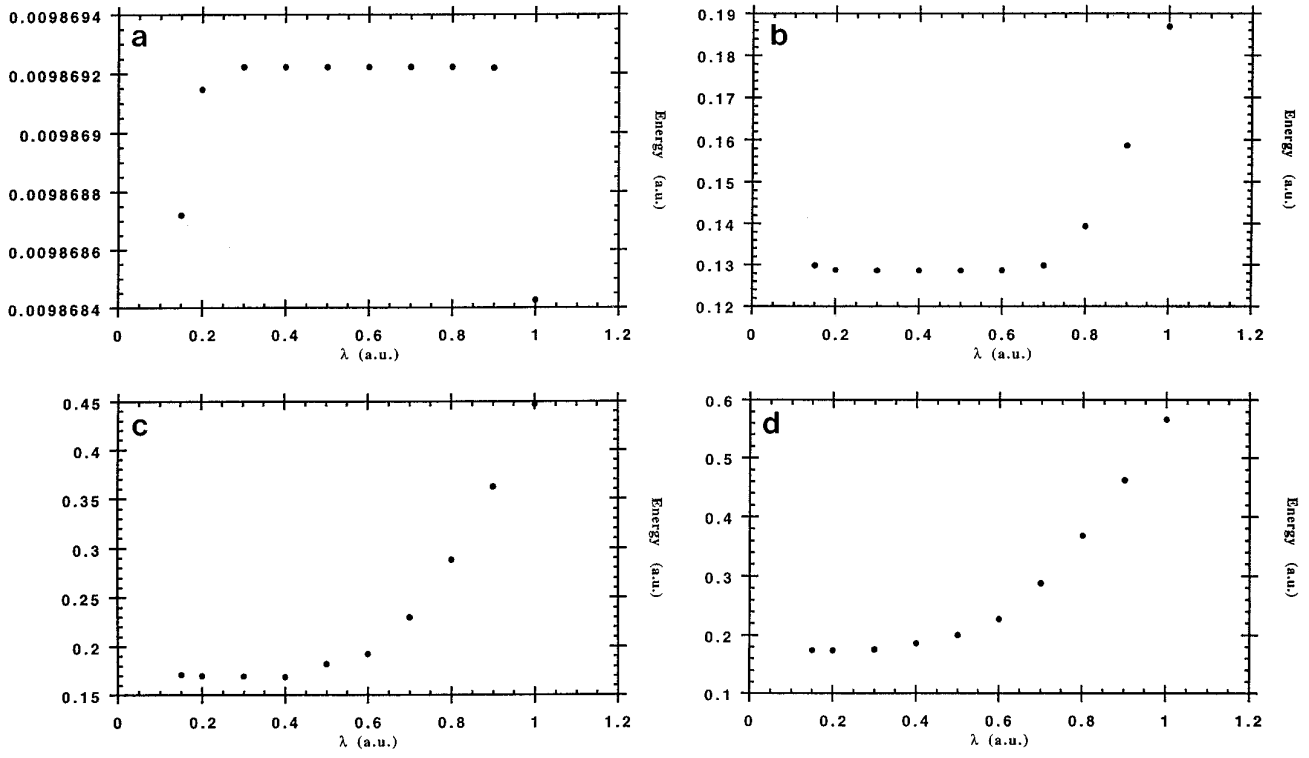

FIG. 2. Energy plots for the $\nu = 0$ (a), 8 (b), 14 (c), and 16 (d) states of the Morse potential versus λ (65 grid points).

$$|L_i[\varphi_j]| \neq 0. \tag{A2}$$

The solution of the interpolation problem is given to $\varphi = \sum_{i=1}^{N} a_i \varphi_i$, where the coefficients a_i are solutions of the system

$$L_i[\varphi_j]a_j = w_i, \tag{A3}$$

(summation on equal indices has been understood).

Now let us consider the following question: how can we approximate a function $f(x)$ defined on an interval I by a function $\varphi(x) \in X$, where X is an N-dimensional space of functions defined on the same interval?

Usually we have certain information about a function, and we must use this information to construct other functions that will approximate it. For example, the ordinary pointwise interpolation is given by

$$L_i[\varphi] \equiv \varphi(x_i) = f(x_i), \tag{A4}$$

where $x_1, x_2, ..., x_N$ are N distinct points lying in I. Pointwise interpolation leads to the construction of a function φ which has the same values of the original function f in N points. This approach can appear to be the most natural for approximating a given function, but this fact does not mean that it is always the most appropriate. For example, a small number of points is not enough to give a good approximation to a rapidly changing function. In this case it could be more useful to know the moments of the function with respect to some set of independent functions $\varphi_1(x)$, $\varphi_2(x)$, ..., $\varphi_N(x)$ in X, i.e.,

$$\tilde{L}_i[\varphi] \equiv \int \varphi(x)\varphi_i(x)\,dx = \int f(x)\varphi_i(x)\,dx. \tag{A5}$$

It is clear that a universal approach to approximating a given function does not exist; the best strategy must be chosen depending on the function we want to approximate.

The situation is even more complex in two dimensions. Here the interpolation could be different for the two independent variables.

Let $g(x, y)$ be a given function defined on S and let $\phi(x, y) \in Y$ be the approximating function, where Y is an $N \times N$-dimensional space of functions on S. Let, finally, the $N \times N$ products of functions $\varphi_i(x)\varphi_j(y)$ be a basis in Y; then we can define the $N \times N$ functionals

$$\tilde{L}_{ij}[\phi] \equiv \int \phi(x_i, y)\varphi_j(y)\,dy = \int g(x_i, y)\varphi_j(y)\,dy. \tag{A6}$$

Obviously

$$\tilde{L}_{ij}[\varphi_k\varphi_h] = L_i[\varphi_k]\tilde{L}_j[\varphi_h], \tag{A7}$$

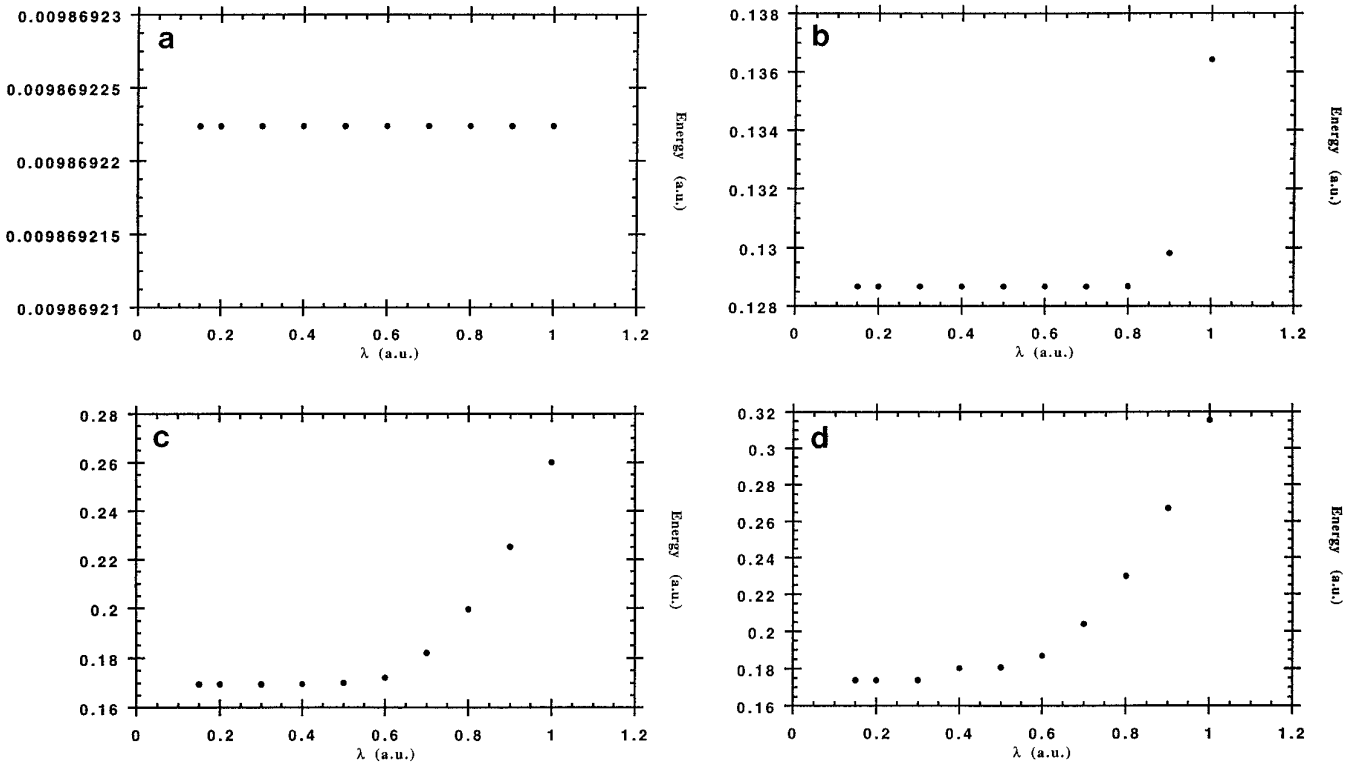

FIG. 3. Energy plots for the $\nu = 0$ (a), 8 (b), 14 (c), and 16 (d) states of the Morse potential versus λ (129 grid points).

where L_i and $\tilde{L}_i$ have been defined previously. This is useful if the function $g(x, y)$ changes rapidly with y for fixed x, but $\int g(x, y)\varphi_i(y)\, dy$ is smooth with respect to x (as in the case of the short time propagator).

Now we have all the ingredients and can prove formally the relations (16) and (22).

Let $\psi(x)$ and $K(x, y; \varepsilon)$ be the wave function and the short time propagator, respectively, and let $\varphi_1(x)$, $\varphi_2(x)$, ..., $\varphi_N(x)$ be our independent expansion functions. Let us define

$$\Phi_{ij} \equiv L_i[\varphi_j], \tag{A8}$$

$$\tilde{\Phi}_{ij} \equiv \tilde{L}_i[\varphi_j]; \tag{A9}$$

then $\psi(x)$ and $K(x, y; \varepsilon)$ can be approximated by

TABLE III

Ground State Energy Values ($\nu = 0$) for the Morse Potential Obtained with Different Time Steps ε

$\varepsilon \times 10^4$ (a.u.)	$N = 65$	$N = 129$
4	0.009869201	0.009869201
2	0.009869218	0.009869218
1	0.009869223	0.009869223
0.5	0.009869226	0.009869224
0	0.009869228	0.009869225
Exact	0.009869224	0.009869224

Note. The value $\varepsilon = 0$ corresponds to a quadratic extrapolation. The last row gives the analytic result. The degree of the Lagrange polynomial is 20. The parameter λ is 0.3 (a.u.).

TABLE IV

Energy Levels $E_{n,l}$ with $l = 0$ of the Pöschl–Teller Radial Potential ($V_0 = 100$)

n	$E^{\text{nu}}_{n,0}$	$E^{\text{th}}_{n,0}$	Relative error
0	19.9763	19.9765	1×10^{-5}
1	43.2781	43.2784	7×10^{-6}
2	62.5800	62.5803	5×10^{-6}
3	77.8818	77.8823	6×10^{-6}
4	89.1838	89.1842	4×10^{-6}
5	96.4860	96.4862	2×10^{-6}
6	99.7885	99.7881	4×10^{-6}

Note. The number of grid points is 30. The numerical and theoretical values of the energy are denoted by $E^{\text{nu}}_{n,0}$ and $E^{\text{th}}_{n,0}$, respectively.

TABLE V

Ground State Energy of the Krazer Potential

A	E_0^{nu}	E_0^{th}	Relative error
5.0	−0.036484	−0.036492	2×10^{-4}
1.0	−0.125716	−0.125000	6×10^{-3}
0.5	−0.191292	−0.190983	2×10^{-3}
0.2	−0.293826	−0.293044	3×10^{-3}

Note. The number of grid points is 30. The Lagrange polynomial degree is 10. The numerical and theoretical values of the energy are denoted by E_0^{nu} and E_0^{th}, respectively.

$$\psi(x) \simeq \Phi_{ij}^{-1}\psi_j \varphi_i(x), \tag{A10}$$

$$K(x, y; \varepsilon) \simeq \Phi_{ij}^{-1}\tilde{\Phi}_{kh}^{-1}\tilde{K}_{jh}^{\varepsilon}\varphi_i(x)\varphi_k(y), \tag{A11}$$

where

$$\psi_i \equiv \psi(x_i), \tag{A12}$$

$$\tilde{K}_{jh}^{\varepsilon} \equiv \int K(x_i, y; \varepsilon)\varphi_j(y)\, dy. \tag{A13}$$

By substituting the expansions (A10) and (A11) into Eq. (4), we obtain

$$\int \Phi_{ij}^{-1}\tilde{\Phi}_{kh}^{-1}\tilde{K}_{jh}^{\varepsilon}\varphi_i(x)\varphi_k(y)\Phi_{lm}^{-1}\psi_m^n\varphi_l(y)dy = e^{-\varepsilon E_n}\Phi_{ij}^{-1}\psi_j^n\varphi_i(x). \tag{A14}$$

The integral yields a factor $\tilde{\Phi}_{kl}$. Therefore, after some simplifications, we get

$$\Phi_{ij}^{-1}\tilde{K}_{jh}^{\varepsilon}\Phi_{hm}^{-1}\psi_m^n\varphi_i(x) = e^{-\varepsilon E_n}\Phi_{ij}^{-1}\psi_j^n\varphi_i(x). \tag{A15}$$

TABLE VI

Ground State Energy of the Krazer Potential with $A = 1$

No. of points	E_0^{nu}	Relative error
30	−0.125716	6×10^{-3}
60	−0.125115	9×10^{-4}
120	−0.125011	9×10^{-5}
E_0^{th}	−0.125000	

Note. The Lagrange polynomial degree is 10. The numerical and theoretical values of the energy are denoted by E_0^{nu} and E_0^{th}, respectively.

TABLE VII

Deuteron Binding Energy

No. of points	E_0[a]
50	−2.224
100	−2.225

Note. The parameter λ is 0.2 fm^{-1}. The Lagrange polynomial degree is 12. The numerical value of the binding energy is denoted by E_0.

[a] $E_{\text{Argonne}} = -2.225$ MeV.

By comparing the coefficients of the various $\varphi_i(x)$, and defining

$$K_{ij}^{\varepsilon} \equiv \Phi_{ih}^{-1}\tilde{K}_{hj}^{\varepsilon}, \tag{A16}$$

$$a_i^n \equiv \Phi_{ij}^{-1}\psi_j^n, \tag{A17}$$

we finally have

$$K_{ij}^{\varepsilon}a_j^n = e^{-\varepsilon E_n}a_i^n. \tag{A18}$$

Thus the eigenvalues of K_{ij}^{ε} are the eigenvalues of the original equation in the approximation given by the expansions (A10) and (A11). Furthermore the $\psi_n(x_i)$ can be obtained from the a_i^n by

$$\psi_n(x_i) = \Phi_{ij}a_j^n. \tag{A19}$$

Thus we have proved Eq. (16). Now, in order to prove Eq. (22), we consider the composition rule (2) and express the propagators by their expansions

$$\Phi_{ij}^{-1}\tilde{\Phi}_{kh}^{-1}\tilde{K}_{jh}^{2\varepsilon}\varphi_i(x)\varphi_k(y) = \int \Phi_{ij}^{-1}\tilde{\Phi}_{kh}^{-1}\tilde{K}_{jh}^{\varepsilon}\varphi_i(x)\varphi_k(z)\Phi_{\alpha\beta}^{-1}\tilde{\Phi}_{\gamma\delta}^{-1}\tilde{K}_{\beta\delta}^{\varepsilon}\varphi_\alpha(z)\varphi_\gamma(y)\, dz. \tag{A20}$$

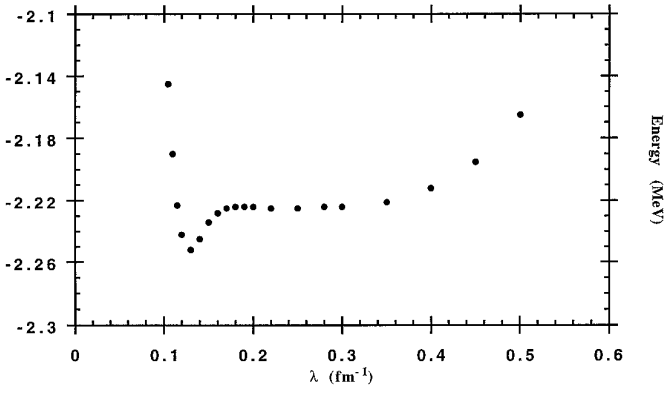

FIG. 4. Energy plot for the ground state of the deuteron versus λ (50 grid points).

By integrating and comparing the coefficients, we obtain

$$K_{ij}^{2\varepsilon} = K_{ih}^{\varepsilon} K_{hj}^{\varepsilon}, \tag{A21}$$

where the matrices K are defined in Eq. (A16). The iteration of this composition rule yields

$$K_{ij}^{T=M\varepsilon} = K_{ih_M}^{\varepsilon} K_{h_M h_{M-1}}^{\varepsilon} \ldots K_{h_1 j}^{\varepsilon}. \tag{A22}$$

Moreover, since

$$K(x, y; \varepsilon) \simeq \tilde{\Phi}_{hj}^{-1} K_{ij}^{T} \varphi_i(x) \varphi_h(y), \tag{A23}$$

we obtain

$$e^{-TE_0} \sim \int K(x, x; T)\, dx \simeq \sum_{i=1}^{N} K_{ii}^{T}, \tag{A24}$$

and

$$e^{-TE_0} \psi^0(x_i) \psi^0(x_j) \sim K(x_i, x_j; T) \simeq \tilde{\Phi}_{hm}^{-1} K_{lm}^{T} \Phi_{il} \Phi_{jm}. \tag{A25}$$

The last equation can be also written as

$$\tilde{\Phi}_{jh}^{-1} K_{ih}^{T} \sim e^{-TE_0} a_i^0 a_j^0. \tag{A26}$$

By using these relations and the Feynman–Kac formula we can obtain the ground state energy and wave function (we need a previous multiplication by $\tilde{\Phi}^{-1}$ to obtain the wave function components a_i).

Finally let us point out that, if we choose a basis $\varphi_i(x)$ such as

$$\varphi_i(x_j) = \delta_{ij}, \tag{A27}$$

which is the case of Section II, we simply have

$$a_i = \psi_i \tag{A28}$$

and

$$K_{ij}^{\varepsilon} = \tilde{K}_{ij}^{\varepsilon}. \tag{A29}$$

Therefore Eqs. (A18) and (A21) reduce to Eqs. (16) and (22), respectively.

ACKNOWLEDGMENTS

I thank F. Iachello, M. Rosa-Clot, and S. Rosati for many helpful discussions and important suggestions and A. Dellafiore for a critical reading of the manuscript.

REFERENCES

1. D. Thirumalai, E. J. Bruskin, and B. J. Berne, *J. Chem. Phys.* **79,** 5063 (1983).
2. C. C. Gerry and J. Kiefer, *Am. J. Phys.* **56,** 1002 (1988).
3. E. Onofri and G. P. Tecchiolli, *Phys. Scripta* **37,** 323 (1988).
4. P. Maraner, E. Onofri, and G. P. Tecchiolli, *J. Comput. Appl. Math.* **37,** 209 (1991).
5. D. C. Khandekar, S. V. Lawande, and K. V. Bhagwat, *Path-Integral Methods and Their Applications* (World Scientific, Singapore, 1993), p. 317.
6. M. Rosa-Clot and S. Taddei, *Phys. Rev. C* **50,** 627 (1994).
7. M. Rosa-Clot and S. Taddei, in *Perspectives on Theoretical Nuclear Physics,* edited by A. Bonaccorso *et al.* (ETS Editrice, Pisa, 1993).
8. M. Rosa-Clot and S. Taddei, *Phys. Lett. A* **197,** 1 (1995).
9. H. De Raedt, *Comput. Phys. Rep.* **7,** 1 (1987).
10. N. Makri, *Chem. Phys. Lett.* **193,** 435 (1992).
11. N. Makri, *J. Phys. Chem.* **97,** 2417 (1993).
12. Y. Huang *et al., J. Chem. Phys.* **99,** 1028 (1993).
13. D. K. Hoffman *et al., J. Chem. Phys.* **99,** 1124 (1993).
14. D. M. Ceperley, *Rev. Mod. Phys.* **67,** 279 (1995).
15. J. W. Negele and H. Orland, *Quantum Many-Particle Systems* (Addison–Wesley, New York, 1988), p. 132.
16. N. Makri and W. H. Miller, *J. Chem. Phys.* **90,** 904 (1989).
17. I. Bender, D. Gromes, and U. Marquard, *Nucl. Phys. B* **346,** 593 (1990).
18. L. S. Schulman, *Techniques and Applications of Path Integration* (Wiley–Interscience, New York, 1981).
19. L. M. Delves and J. Walsh, *Numerical Solution of Integral Equations* (Clarendon Press, Oxford, 1974), p. 80.
20. C. Lanczos, *J. Res. Nat. Bur. Standards* **45,** 255 (1950).
21. H. Kleinert, *Path-Integrals in Quantum Mechanics Statistics and Polymer Physics* (World Scientific, Singapore, 1990), p. 251.
22. N. W. Schellingerhout, L. P. Kok, and G. D. Bosveld, *Phys. Rev. A* **40,** 5568 (1989).
23. C. C. Marston and G. G. Balint-Kurti, *J. Chem. Phys.* **91,** 3571 (1989).
24. J. C. Light, I. P. Hamilton, and J. V. Lill, *J. Chem. Phys.* **82,** 1400 (1985).
25. R. B. Wiringa, R. A. Smith, and T. L. Ainsworth, *Phys. Rev. C* **29,** 1207 (1984).
26. A. Kievsky, M. Viviani, and S. Rosati, in *Perspectives on Theoretical Nuclear Physics,* edited by L. Bracci *et al.* (ETS Editrice, Pisa, 1989).
27. P. J. Davis, *Interpolation and Approximation* (Blaisdell Pub., New York, 1963), p. 24.